The Design of Multi Band Antenna with Improved Higher order mode Radiation Using CMA for L5-band, L1-band, and S-band Application

Indra Bhooshan Sharma [1$, *], Prachi Joshi [2$], Subhash Shrimal[3$], Bhawna Kalra[4$], and M. M. Sharma[5$]
[$]Department of ECE, Malaviya National Institute of Technology, Jaipur, India-302017
*Corresponding Author Mobile Number - +91-9511595262
[1]2019rec9064@mnit.ac.in, [2]2022pec5179@mnit.ac.in, [3]2019rec9534@mnit.ac.in, [4]2019rec9507@mnit.ac.in, [5]mms.ece@mnit.ac.in
1. *Present Adress: Department of ECE, Malaviya National Institute of Technology, JLN Marg Jaipur, India-302017*

Abstract: A novel multi-band antenna with an improved higher-order mode radiation pattern based on characteristic mode analysis (CMA) is presented. The tri-band characteristic is achieved by exciting one higher-order mode and two orthogonal modes. The initial orthogonal mode is achieved by converting the antenna from a circular to an elliptical shape. Surface current reshaping transforms the higher-order conical radiation pattern mode into a broadside direction. The surface current nulls with out-of-phase are moved toward the patch corners using CMA. Characteristic modes excite with coaxial feed, which uses full-wave EM simulation. It excites two orthogonal modes at 1176 MHz, 1575 MHz for L5-band and L1-band applications respectively, and one higher-order mode at 2500 MHz for S-band applications. The proposed antenna has moderate gain and broadside radiation patterns across the operational frequency bands. The working of the antenna and validation are represented by equivalent circuit modeling. The experimental results present excellent agreement with EM simulated results.

Keywords: Characteristic Mode Analysis, L1-band, L5-band, orthogonal modes, S-band, Tri-band antenna.

1. Introduction

The space communication and radar applications require multi-band antennas with broadside radiation characteristics for better signal coverage. Microstrip antennas are frequently used in multi-band applications with appealing abilities, including their low price, low profile, less heaviness, and effortlessness of circuit integration [1, 2]. Multi-band antennas are commonly designed using stacked multi-resonators, slots, and planar inverted antennas. The multi-resonators, stacked antenna enhances the lateral dimension or height. The methods used, such as shorting pins, etched slots, and adding extra parasitic components, are responsible for distorted radiation patterns and high cross-polarization [3, 4].

The higher-order modes are the best solution for a multi-band and thin-profile antenna. The fundamental mode is radiated in a broadside direction, but higher-order mode radiation patterns cannot maintain a broadside direction and have high E-plane side lobes [5]. Therefore, we require proper methods to convert higher-order modes radiation patterns in the broadside direction for multi-band applications.

The three methods are discussed in [2] to convert higher ordering mode radiation patterns in broadside and minimize E-plane side lobs. The first method is to partially load metamaterial in patches to change conical to the broadside radiation pattern. However, in these methods, the antenna's fabrication complexity is high. The second method is adding reflectors with antenna structure. This method also increases antenna volume and is unreliable in integration with planar circuits. In the third method, there are controlling field distributions in the antenna structure with higher-order modes to maintain broadside radiation patterns. Some literature is available based on a third method, such as inserting a non-resonant slot at the patch center to diminish the E-plane side lobes of TM_{12} mode [6]-[8]. The higher-order radiation pattern of the patch is transformed into the broadside direction using a differential fed with the etching center slot of the patch discussed in [1, 4]. In the equivalent magnetic current magnitudes are controlled to convert the higher-order mode from conical to broadside radiation pattern by utilizing port feeding along with shorting pins and slots [2]. However, these techniques enhance circuit complexity by loading slots and pins with differential feeding. So, to overcome the antenna's complexity and radiation characteristics of higher ordering mode, the antenna structure is modified [9]-[20]. The broadside radiation pattern is obtained by shifting out-of-phase surface current nulls toward the patch corners. This paper presents a new technique for refining the antenna radiation pattern of the higher-order mode from conical to broadside. The three-band characteristics are accomplished by re-allocating one higher-order mode (TM_{12}) at the S-band and two orthogonal modes (TM_{11H}, TM_{11V}) at L5-band and L1-band by using re-shaping of the circular patch antenna. The mode analysis method provides the structurally dependent modes.

2. Design Considerations of Tri-band Antenna

2.1. Cavity Model Method Based Modal Analysis

Cavity model method (CMM) is an analytical method for understanding conventional microstrip antenna characteristics with vital assumptions. But, it is hard to comprehend irregular-shaped microstrip antennas. The circular cavity model exhibits some resonance modes.

For TM^{Z}_{mno} mode, the resonance frequency is given as:

$$(f_r)_{mn0} = \frac{c}{2\pi\sqrt{\varepsilon_r}}\left(\frac{\chi'_{mn}}{R}\right) \tag{1}$$

Where 'R' denotes the circular patch radius shown in Figure 1, 'c' is free space light speed, ε_r is relative permittivity of substrate and χ'_{mn} determines the resonant frequency order. At $\chi'_{11} = 1.8412$ for first-order mode $\left(TM^{Z}_{110}\right)$ and $\chi'_{12} = 3.0542$ for second-order mode $\left(TM^{Z}_{120}\right)$.

Equation (1) can be used to calculate the R parameter of a circular patch antenna. The proposed antenna is designed by *FR-4* substrate with ε_r=4.3 and tanδ = 0.025. Its lower frequency for the first-order mode is 1176 MHz (TM^{Z}_{110}). The parameter is calculated as given below:

1. $R = \dfrac{1.8412 * 3 * 10^{8}}{2\pi * 1176.45 * 10^{6}\sqrt{4.3}} = 36.05\,mm,$

Using R and equation (1), we can calculate second-order mode TM^{Z}_{120} frequency as

2. $(f_r)_{120} = \dfrac{3.0542 * 3 * 10^{8}}{2\pi * 36.05 * 10^{-3}\sqrt{4.3}} = 1951.72\,MH_Z.$

2.2. Antenna Re-shaping using CMA

2.2.1. Brief Introduction of CMA theory

The usual mode analysis method is widely utilized in microwave circuit design. It provides step-by-step systematic design analysis and in-depth physical mode behavior in conducting structures. The CMA is based on Method of Moments (MoM) and characteristic modes can be numerically calculated for any arbitrary shape of conducting structure [21]-[26]. The following factors are required for performing modal analysis of conducting systems.

1. **Eigenvalue** λ_n **:** The Eigenvalue for the n^{th}mode denotes the ratio of near-structure energy storage $P_{reac,n}$ to radiated energy $P_{rad,n}$ [27]:

$$\lambda_n = \frac{< J_n^* X(J_n) >}{< J_n^* R(J_n) >} = \frac{P_{reac,n}}{P_{rad,n}} \qquad (2)$$

Where J_n (* stands for the conjugate operator) is characteristics current and R and X are corresponding impedance matrix's real and imaginary components of conducting body.
The properties of eigenvalues given as [28]-[31]:

(1) $\lambda_n > 0$, mode is inductive and stores magnetic energy.

(2) $\lambda_n < 0$, mode is capacitive and stores electric energy.

(3) $\lambda_n = 0$, mode is in resonance.

2. Modal Significance (MS_n): MS_n is another crucial parameter for representing the mode's radiation characteristics. It is defined as [32]

$$MS = \left| \frac{1}{1 + j\lambda_n} \right| \qquad (3)$$

When $MS_n > \frac{1}{\sqrt{2}}$, then it is significant for radiating mode and vice versa.

The coupling behavior of the nth characteristic mode and excitation (feed excitation) is represented as input admittance (Y_{in}) with current (I_{in}) and voltage (V_{in}) at the feed location [33].

$$Y_{in} = \frac{I_{in}}{V_{in}} = \sum \frac{(j_n^p)^2}{1 + j\lambda_n} \qquad (4)$$

Where J_n^p the nth characteristic mode current impedance and the appropriate reflection coefficient (Γ_n) is are provided below. Excited by feed with Z_o characteristic impedance.

$$\Gamma_n = \frac{\left(\frac{1}{Y_{in}^n}\right) - Z_0}{\left(\frac{1}{Y_{in}^n}\right) + Z_0} \qquad (5)$$

2.2.2 Antenna-1 modal analysis with parametric study

The working principle of a tri-band antenna with higher-order mode radiation characteristic enhancement is demonstrated by surface current distribution and radiation pattern analysis using the CMA method. The design and simulation are carried out by the CST Studio EM tool.
In this step, the initial circular patch antenna is designed using a calculated parameter R=36.05 mm through the CMM, as shown in figure 2(a). Figure 3(a) depicts the MS_n values plot for four modes of antenna-1 with distinct values of R (34.50 mm, 35.5 mm, and 36.50 mm). In this plot, modes 1, 2, and 4

are resonated because their MS_n values are more significant than $MS_n > \frac{1}{\sqrt{2}}$. The mode-3 is not resonant, and it stores magnetic energy due to $\lambda_3 > 0$, while λ_1 (for mode-1), λ_2 (for mode-2) are zero at 1176 MHz, and λ_4 (for mode-4) is zero at 2004 MHz as in depicted figure 3(b).

Mode-1 and 2 are orthogonal (TM_{11H} & TM_{11V}) and overlapped at the same frequency, but mode-4 is a higher-order mode (TM_{12}). At R=35.50 mm, the antenna is resonant at 1176 MHz (due to TM_{11H} & TM_{11V}) and 2004 MHz (due to TM_{12}). The working mechanism of antenna-1 can be intuitively understood by looking at the surface current and the radiation pattern, as revealed in Figure 4(a-d) and Figure 5(a-d), respectively. The mode-1 and 2 have orthogonal radiation pattern to each other because the arrows of surface currents are 90^{o} shifted to each other. The broadside radiation pattern of each mode is due to arrows of surface currents distributed in phase. The mode-3 behaves inductively owing to its arrows of surface currents being in a closed loop, which is verified by the eigenvalue plot in Figure 3(b). The radiation pattern of mode-4 is a conical shape owing to the surface out-of-phase current arrows at middle of the patch. Figure 3 illustrates a detailed analysis centered on antenna-1, with the primary goal of extracting the modal properties associated with specific circular patch dimensions. The analysis was conducted without any excitation, and it covered up to four different modes for antenna-1. These results were obtained using the CST Studio's CMA analysis software tool.

2.2.3 Antenna-2 modal analysis with parametric study

The circular patch antenna is transformed into an elliptical shape using parametric analysis, as shown in Figure 2 (b). The orthogonal modes were separated by parametric study at 1176 MHz and 1575 MHz (L1-band) with R_x=35.5 mm and R_y=25.5 mm, and higher-order mode-4 is located at 2150 MHz as in Figure 6. Radiation pattern remains unchanged for modes 1, 2, and 3 due to similar surface current distribution as discussed in the circular-shaped antenna-1. Still, the radiation pattern for mode-4 is dramatically changed due to changing surface current in the elliptical-shaped antenna as shown in Figure 4(e-h) and it's corresponding far-field shown in Figure 5(e-h). In this step, the desirable mode-1 at 1176 MHz and mode-2 at 1575 MHz are achieved, and further, the antenna needs to re-shape for the S-band to achieve tri-band characteristics.

2.2.4 Antenna-3 modal analysis with parametric study

The elliptical-shaped antenna-2 is re-shaped with parameter $\theta 1$, as shown in Figure 2(c). The parametric study with different $\theta 1$ (85^0, 95^0, and 105^0) of antenna-3 as shown in Figure 7. At $\theta 1$=95^0, the mode-1, 2, and 4 are resonated (due to $MS_n > \frac{1}{\sqrt{2}}$) for 1176 MHz, 1575 MHz, and 2500 MHz frequency bands, but mode-3 is not resonant (due to MS_n=0), and behaves inductively as stores magnetic energy. This step realizes the tri-band characteristics for L5, L1, and S-band applications, respectively. The orthogonal modes (mode-1, 2) radiation patterns are in the broadside direction due to in-phase surface current distribution. Still, the radiation pattern of mode-4 is not in the broadside direction due to the availability of out-of-phase surface currents nulls in the center, as shown in Figure 4(i-l) and the corresponding far-field shown in Figure 5(i-l). The mode-4 at 2500 MHz for S-band is not desirable for broadside coverage because of the E-plane show high level of adjacent lobes. This problem can be fixed further by altering the antenna design. So, the corner sides of the antenna construction get surface out-of-phase current nulls.

2.2.5 Antenna-4 modal analysis with parametric study

In this step, the antenna-3 is further re-shaped with the new parameter $R1$ and $\theta 2$ to convert the broadside radiation pattern of higher-order mode-4 as shown in Figure 2 (d). Figure 4 and Figure 5 show parametric study plots of parameters $R1$ and $\theta 2$ with different values. Using surface currents and radiation patterns study, the new parameters ($R1$ & $\theta 2$) are varied. So, the broadside radiation pattern of mode-4 is achieved while maintaining stable desired frequency bands. Figure 8 shows the Antenna-4 modal analysis. At $R1$=11.33 mm and $\theta 2=72^0$, the radiation patterns of mode-4 are in a broadside direction. Because, there are no out-of-phase surface currents null in the center of the patch are similar for mode-1 and mode-2 in the broadside direction as shown in Figures 7(m-p) and Figures 8(m-p). The process for converting the broadside radiation pattern of a higher-order mode along with orthogonal modes is well presented in far-field plots with the $\phi = 90^0$ and $\phi = 0^0$ as represented in Figure 9 and 10.

2.3. Tri-Band Antenna in Full Wave with Excitation

Figure 11 depicts the optimized tri-band antenna geometry with coaxial feed. The desired characteristics modes are excited by parametric study of coaxial feed location (x_o, y_o) in full-wave FIT simulation, as shown in Figure 12. In this Figure, the mode-1, 2 and 4 are excited separately and simultaneously with different feed locations at x_o=-20.93 mm, y_0=9.33 mm and excited simultaneously at 1179 MHz, 1580 MHz, and 2488 MHz.

2.4. Experimental Validation of Proposed Antenna

Figure 13 illustrates the fabricated layout of the antenna. The S_{11} parameter of design is tested in an anechoic chamber, and radiation patterns are analyzed using a vector network analyzer, as shown in Figure 14. The S_{11} parameter comparison results between CST EM-tool and measured by VNA are depicted in Figure 15. Figure 16 illustrates measured peak gain is more significant than 4.9 dBi in all desired bands. The simulated and measurement results have a slight difference due to fabrication tolerance and measurement error. Figure 17 shows the antenna co-polarization ("solid lines" for simulated and "dash lines" for measurement) and cross-polarization ("dotted lines" for simulated and "dash-dot lines" for measurement) along with measurement results with E ($\phi = 90^0$) and H ($\phi = 0^0$) plane. The simulated and measured cross-polarization patterns are below -19dB in the broadside direction for each band. So, antenna has decent isolation between co and cross-polarization for all desired bands. With only slight variations resulting from the measuring environment and manufacturing faults, the measurements' results are quite similar to those of the simulation.

3. The antenna ECM design

The equivalent circuit modelling (ECM) of the proposed antenna is represented in figure 18. In this, the tri-band antenna is represented by three parallel RLC circuits. Mode-1, 2, and 4 are represented by R_1-L_1-C_1, R_2-L_2-C_2, and R_3-L_3-C_3, respectively, as shown in Figure 18(a). These modes are triggered by 50 Port. The port is coupled to these three RLC circuits through L_o, C_o coupling, an inductor, and a capacitor. The ECM is simulated in CST circuit simulation, which optimizes the circuit parameters according to the S_{11} characteristic as exposed in Figure 18(b). Figure 15 displays the validation of the S_{11} from equivalent circuit simulation with simulated full wave simulation and measurement results.

4. Analysis of the Proposed Work concerning the Existing Work

The comparisons with similar work are listed in Table 1. In [1], short pins and slots are employed to generate the dual-band characteristic, and a narrow slot with a differential feed is used to enhance higher-order modes. A similar method is discussed in [5] for the tri-band antenna with higher-order mode enhancement. The structures' complexity is high in both cases regarding fabrication. The higher-order mode enhancement is achieved by placing a narrow slot at the patch center, as reported in [4, 6] for dual and single-band antenna. The dual-band antenna characteristic is achieved in [2] by exciting TM_{010} and TM_{030} modes, and putting double-negative (DNG) or mu-negative (MNG) metamaterial is utilized to enhance the higher-order mode radiation pattern. This paper proposes a new approach to improving higher mode radiation pattern antenna by modifying antenna design. The modified antenna design obtains the surface out-of-phase current nulls toward the patch corners with exciting two orthogonal modes and one higher-ordering mode for tri-band applications [33]-[35].

5. Conclusion

In this paper, a new approach is used to design and analyze a tri-band antenna to enhance higher-order mode radiation characteristics using characteristic mode analysis. The two orthogonally modes at the L5, L1 bands and one higher ordering mode at S-band are reallocated to obtain the tri-band characteristic. The radiation characteristics of the higher mode are enhanced by shifting the surface current nulls. It is modifying the antenna structure with out-of-phase nulls toward the patch corners. The designed antenna fabrication complexity is relatively low compared to earlier literature. The slots, shorting pins, or differential feed have not been used in the designed antenna. Only re-shaped the antenna structure obtains multiband antenna characteristics. The final antenna design was fabricated on low-cost *FR-4* material, and the S_{11} parameter and radiation patterns were tested. The measurement results are nearly identical to the EM simulation results. The designed antenna's resonance frequencies are 1182 MHz, 1585 MHz, and 2500 MHz, and it has sufficient gain and a broadside radiation pattern for Global Positioning System (GPS) application as the L1-band and Indian Regional Navigation Satellite System (IRNSS) application as both L5 and S-band.

References

[1] Zhang, X. and Zhu, L. "Dual-band high-gain differentially fed circular patch antenna working in TM11 and TM12 modes," in *IEEE Transactions on Antennas and Propagation*, **66** (6), pp. 3160-3165, (2018).

[2] Liu, X., Li, Y., Liang, Z., and et al. "A gain-enhanced tri-band microstrip square antenna with consistent radiation patterns by manipulating its higher order modes," in *IEEE Transactions on Antennas and Propagation*, **67** (3), pp. 1987-1992, (2019).

[3] Xiong, J., Li, H., Jin, Y., and et al. "Modified TM_{020} mode of a rectangular patch antenna partially loaded with metamaterial for dual-band applications," in *IEEE Antennas and Wireless Propagation Letters*, **8**, pp. 1006-1009, (2009).

[4] Hoang, T.-V., Le, T.-T., Li, Q. Y., and et al. "Quad-band circularly polarized antenna for 2.4/5.3/5.8-GHz WLAN and 3.5-GHz WiMAX applications," in *IEEE Antennas and Wireless Propagation Letters*, **15**, pp. 1032-1035, (2016).

[5] Liu, N.-W., Zhu, L., Zhang, X. and et al. "A wideband differential-fed dual-polarized microstrip antenna under radiation of dual improved odd-order resonant modes," in *IEEE Access*, **5**, pp. 23672-23680, (2017).

[6] Juyal, P. and Shafai, L. "Side lobe reduction of TM12 mode of circular patch via non resonant narrow slot," in *IEEE Transactions on Antennas and Propagation,* **64**(8), pp. 3361-3369, (2016).

[7] Balanis, C.A., "*Antenna Theory-Analysis and Design*," John Wiley & Sons.,**170**, pp. 811-872 (2010).

[8] Yan, Y., Sharif, A., Ouyang, J., and et al. "UHF RFID handset antenna design with slant polarization for IoT and future 5G enabled smart cities applications using CM analysis," in *IEEE Access*, **8**, pp. 22792-22801, (2020).

[9] Feng, B., Chen, J. and Sim, C.-Y.-D. "Analysis of double-xi-shaped millimetre-wave patch antenna backed by a high-order-mode cavity using characteristic mode design", *IET Microwave Antennas Propagation*, **15** (8), pp. 966-980, (2021).

[10] Yinusa, K.-A., Marcos, E.-P. and Caizzone, S. "Robust satellite navigation by means of a spherical cap conformal antenna array," *2018 18th International Symposium on Antenna Technology and Applied Electromagnetics (ANTEM)*, Waterloo, ON, Canada, pp. 1-2, (2018).

[11] Yen, S., Boskovic, L. B., Friedrichs, G. R. and et al., "Fast prototyping of an L-band array using additive and subtractive techniques," *2023 International Workshop on Antenna Technology (iWAT),* Aalborg, Denmark, pp. 1-4, (2023).

[12] De Araújo, J.-B., Morales, C. D., Morlaas C. and et al. "A dual-band hollow dielectric resonator antenna for GPS applications," *2021 IEEE International Symposium on Antennas and Propagation and USNC-URSI Radio Science Meeting (APS/URSI),* Singapore, Singapore, pp. 1177-1178, (2021).

[13] Chaudhary, P., Ghodgaonkar, D.-K., Gupta, S. and et al., "Miniaturized L1 and L5-band circularly polarized rectangular dielectric resonator antennas for navigation satellite applications," *2021 IEEE Indian Conference on Antennas and Propagation (InCAP)*, India, pp. 340-343, (2021).

[14] Wang, N., Wang, J., Xu, T. and et al. "Applications of ground-based multipath reflectometry based on combinations of pseudorange and carrier phase observations of multi-GNSS dual-frequency signals," *in IEEE Journal of Selected Topics in Applied Earth Observations and Remote Sensing*, **14**, pp. 9557-9570, (2021).

[15] Honnaiah, P.-J., Maturo, N., Chatzinotas, S. and et al. "Demand-based adaptive multi-beam pattern and footprint planning for high throughput GEO satellite systems," in *IEEE Open Journal of the Communications Society*, **2**, pp. 1526-1540, (2021).

[16] Saeidi, T. and Zadeh, S.-K. "A miniaturized multi-frequency wide-band leaky wave button antenna for ISM/5G communications and WBAN applications," *in Radio Science*, **58**(3), pp. 1-18, (2023).

[17] Hwang, M., Kim, G., Kim, J. and et al. "A simultaneous beam steering and polarization converting S-band transmit array antenna," *in IEEE Access*, **10**, pp. 105111-105119, (2022).

[18] Roy, S., Tiang, R.-J.-J., Roslee, M. B., and et al. "Quad-band multiport rectenna for RF energy harvesting in ambient environment," *in IEEE Access*, **9**, pp. 77464-77481, (2021).

[19] Xiao, Y., Lu, W. J., Zhao, M. L. and et al. "Triple-mode resonant backfire feed antenna with nearly equal E-/H-plane and inverse taper patterns," *in IEEE Transactions on Circuits and Systems II: Express Briefs*, **70**(6), pp. 1946-1950, (2023).

[20] Khan, A., He, Y., He, Z. and et al. "A compact quadruple-band circular polarized MIMO antenna with low mutual coupling," *in IEEE Transactions on Circuits and Systems II: Express Briefs*, **70**(2), pp. 501-505, (2023).

[21] Feng, B., Yang, B., Sim, C.-Y.-D. and et al. "A compact vehicle-mounted garden-themed artistic antenna with isolation improvement for 2G/3G/LTE/5G sub-6-GHz/WiFi/Bluetooth Communications," *in IEEE Transactions on Vehicular Technology*, 72(4), pp. 4851-4862, (2023).

[22] Dong, J., Wang, S. and Mo, J. "Design of a twelve-port MIMO antenna system for multi-mode 4G/5G smartphone applications based on characteristic mode analysis," *in IEEE Access*, **8**, pp. 90751-90759, (2020).

[23] Q. Wu, "Characteristic mode assisted design of dielectric resonator antennas with feedings," *in IEEE Transactions on Antennas and Propagation*, **67**(8), pp. 5294-5304, (2019).

[24] Che, J.-K., Chen, C.-C. and Locke, J.-F. "A compact cavity-backed tri-band antenna design for flush mount GNSS (L1/L5) and SDARS operations," *in IEEE Antennas and Wireless Propagation Letters*, **20**(5), pp. 638-642, (2021).

[25] Li, H., Du, J., Yang, X.-X. and et al. "Low-profile all-textile multiband microstrip circular patch antenna for WBAN applications," *in IEEE Antennas and Wireless Propagation Letters*, **21**(4), pp. 779-783, (2022).
[26] Awais, M., Madni, A. and Khan, W. T. "Design of a compact high isolation 4-element wideband patch antenna array for GNSS applications," *in IEEE Access*, **10**, pp. 13780-13786, (2022).
[27] Zhang, Q., Ma, R., Su, W., and et al. "Design of a multimode UWB antenna using characteristic mode analysis," *in IEEE Transactions on Antennas and Propagation*, **66**(7), pp. 3712-3717, (2018).
[28] Al-Mihrab, M.-A., Salim, A.-J. and Ali, J.-K. "A compact multiband printed monopole antenna with hybrid polarization radiation for GPS, LTE, and Satellite applications," *in IEEE Access*, **8**, pp. 110371-110380, (2020).
[29] Liu, N.-W., Zhu, L. Liu, Z.-X. and et al. "Radiation pattern reshaping of a narrow slot antenna for bandwidth enhancement and stable pattern using characteristic modes analysis," *in IEEE Transactions on Antennas and Propagation*, **70**(1), pp. 726-731, (2022).
[30] Deng, C., Zhao, Z. and Yu, W. "Characteristic mode analysis of circular microstrip patch antenna and its application to pattern diversity design," *in IEEE Access*, **10**, pp. 2399-2407, (2022).
[31] Zeng, J., Liang, X., He, L. and et al. "Single-fed triple-mode wideband circularly polarized microstrip antennas using characteristic mode analysis," *in IEEE Transactions on Antennas and Propagation*, **70**(2), pp. 846-855, (2022).
[32] Han, M. and Dou, W. "Compact clock-shaped broadband circularly polarized antenna based on characteristic mode analysis," in *IEEE Access*, **7**, pp. 159952-159959, (2019).
[33] Kumar, A., Deegwal, J.-K., and Sharma, M.-M. “Miniaturized multi stubs loaded rectangular monopole antenna for multiband applications based on theory of characteristics modes,” in *Progress In Electromagnetics Research C*, 92, 177-189, (2019).
[34] Sharif, A., Ouyang, J., Raza, A., and et al. "UHF RFID tag design using theory of characteristics modes for platform-tolerant and harsh metallic environments," in *IEEE Journal of Radio Frequency Identification*, **6**, pp. 524-533, (2022).
[35] Zhang, Q. and Gao, Y. “Compact low-profile UWB antenna with characteristic mode analysis for UHF TV white space devices” *IET Microwaves, Antennas & Propagation*, **11**(11), pp. 1629 – 1635, (2017).

Figures Captions List
Figure 1. Dielectric-loaded circular patch antenna.
(a) Antenna-1 **(b)** Antenna-2 **(c)** Antenna-3 **(d)** Antenna-4
Figure 2. Proposed antenna design steps geometries
(a) Antenna-1 parametric study MS plot **(b)** Eigen value plot
Figure 3. Antenna-1 modal analysis
Figure 4. Surface currents distribution of antennas
Figure 5. Far-field radiation patterns of antennas
Figure 6. Antenna-2 parametric study MS plot
Figure 7. Antenna-3 parametric study MS plot
(a) Antenna-4 parametric study MS plot with *R1* **(b)** Antenna-4 parametric study MS plot with $\theta 2$
Figure 8. Antenna-4 modal analysis

(a) Mode-1 **(b)** Mode-2 **(c)** Mode-3 **(d)** Mode-4
Figure 9. Farfield radiation characteristics at Phi=0
(a) Mode-1 **(b)** Mode-2 **(c)** Mode-3 (**d)** Mode-4
Figure 10. Far field radiation characteristics at Phi=90
Figure11. Geometry of proposed tri-band antenna
Figure 12. S_{11} plot for modes excitation with feed
Figure 13. Photograph of the fabricated layout of
Figure 14. S_{11} and radiation pattern measurement set-up of proposed antenna the proposed antenna
Figure 15**.** Scattering Parameter (S_{11}) of antenna
Figure 16. Simulated and measured peak gain
(a) $\phi = 90^0$, 1174 MHz **(b)** $\phi = 90^0$, 1575 MHz **(c)** $\phi = 90^0$, 2495 MHz **(d)** $\phi = 0^0$, 1174 MHz **(e)** $\phi = 0^0$, 1575 MHz **(f)** $\phi = 0^0$, 2495 MHz
Figure 17. The proposed antenna's measured and simulation-based radiation pattern {Solid line Co-pol (——— Simulated), Dash line Co-pol (– – – – Measured), Square dot line Cross-pol (·········· Simulated), Dash Dot Cross line pol (– · – · – Measured)}
Figure 18. (a) Equivalent Circuit Modeling (ECM) analysis (b) S_{11} of ECM of proposed antenna

Table Captions List

TABLE 1 Comparison of proposed approach with previous work.

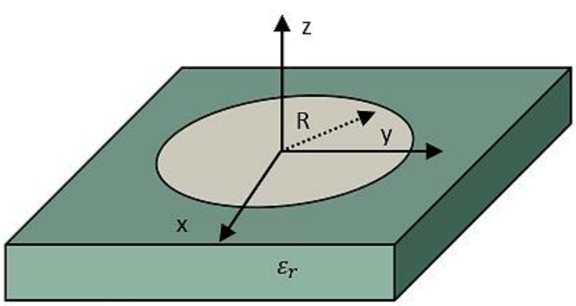

Figure 1. Dielectric-loaded circular patch antenna.

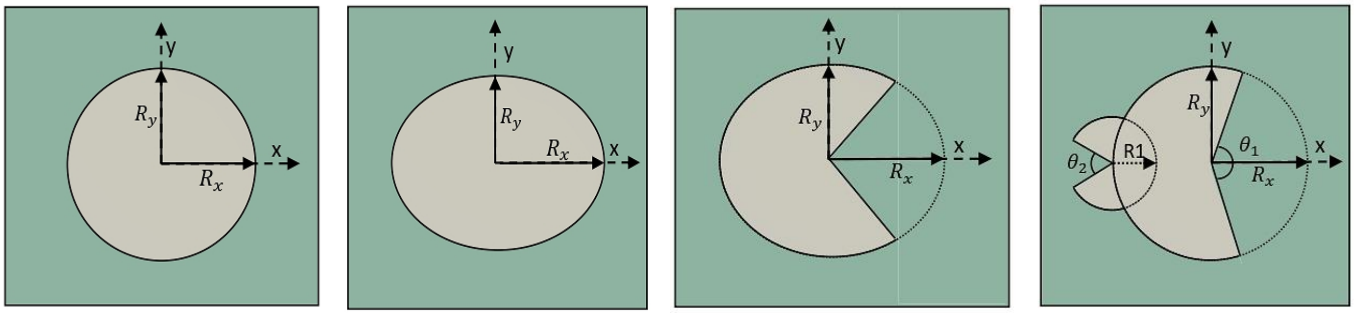

(a) Antenna-1 (**b)** Antenna-2 **(c)** Antenna-3 **(d)** Antenna-4

Figure 2. Proposed antenna design steps geometries

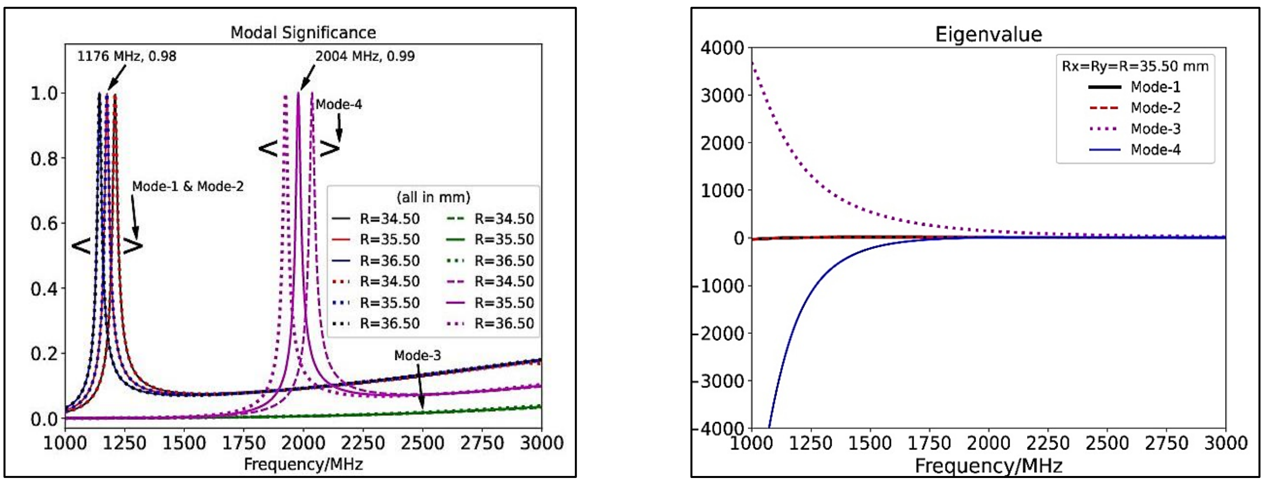

(a) Antenna-1 parametric study MS plot (**b)** Eigen value plot

Figure 3. Antenna-1 modal analysis

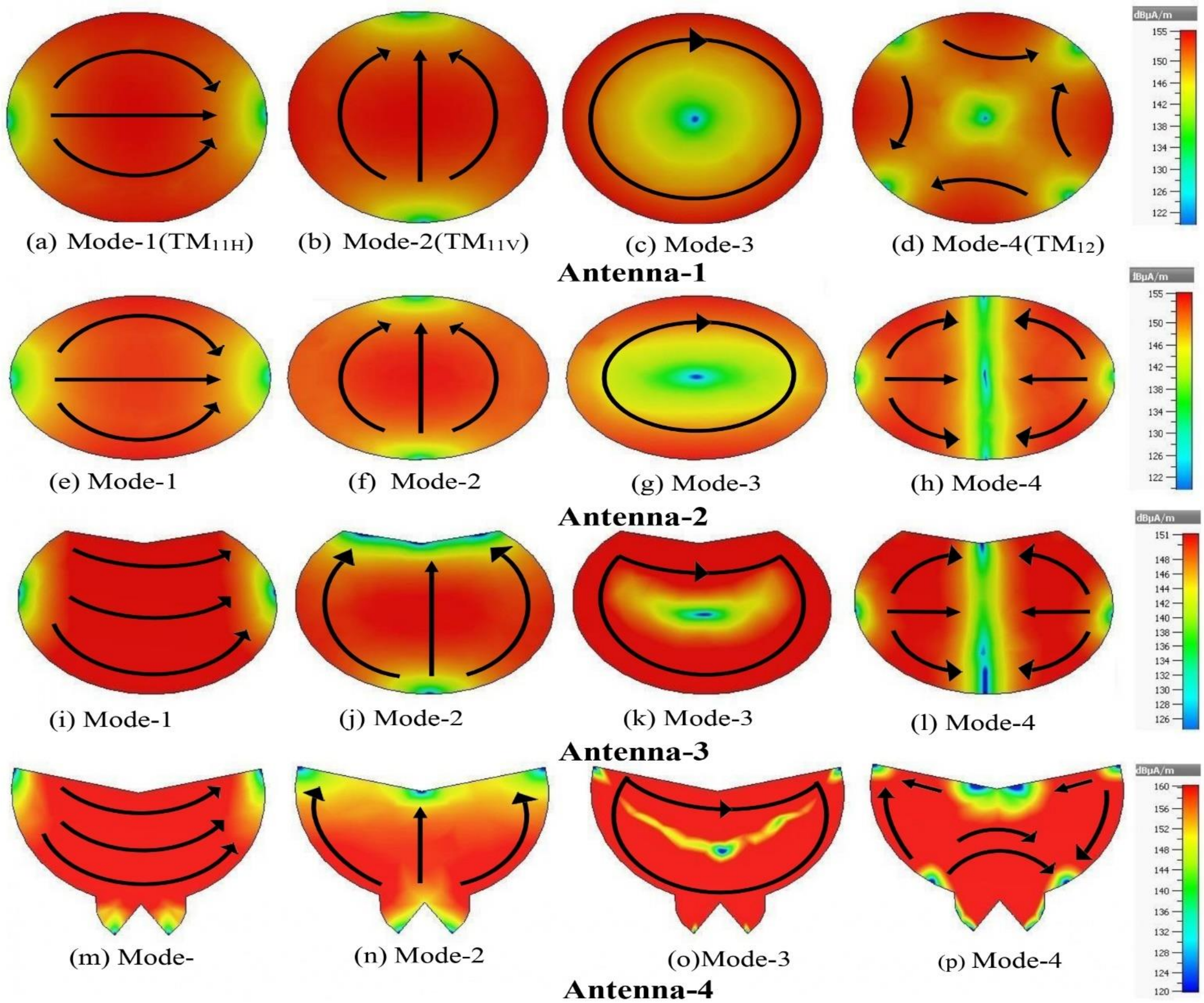

Figure 4. Surface currents distribution of antennas
(Solid arrows show the direction of surface currents)

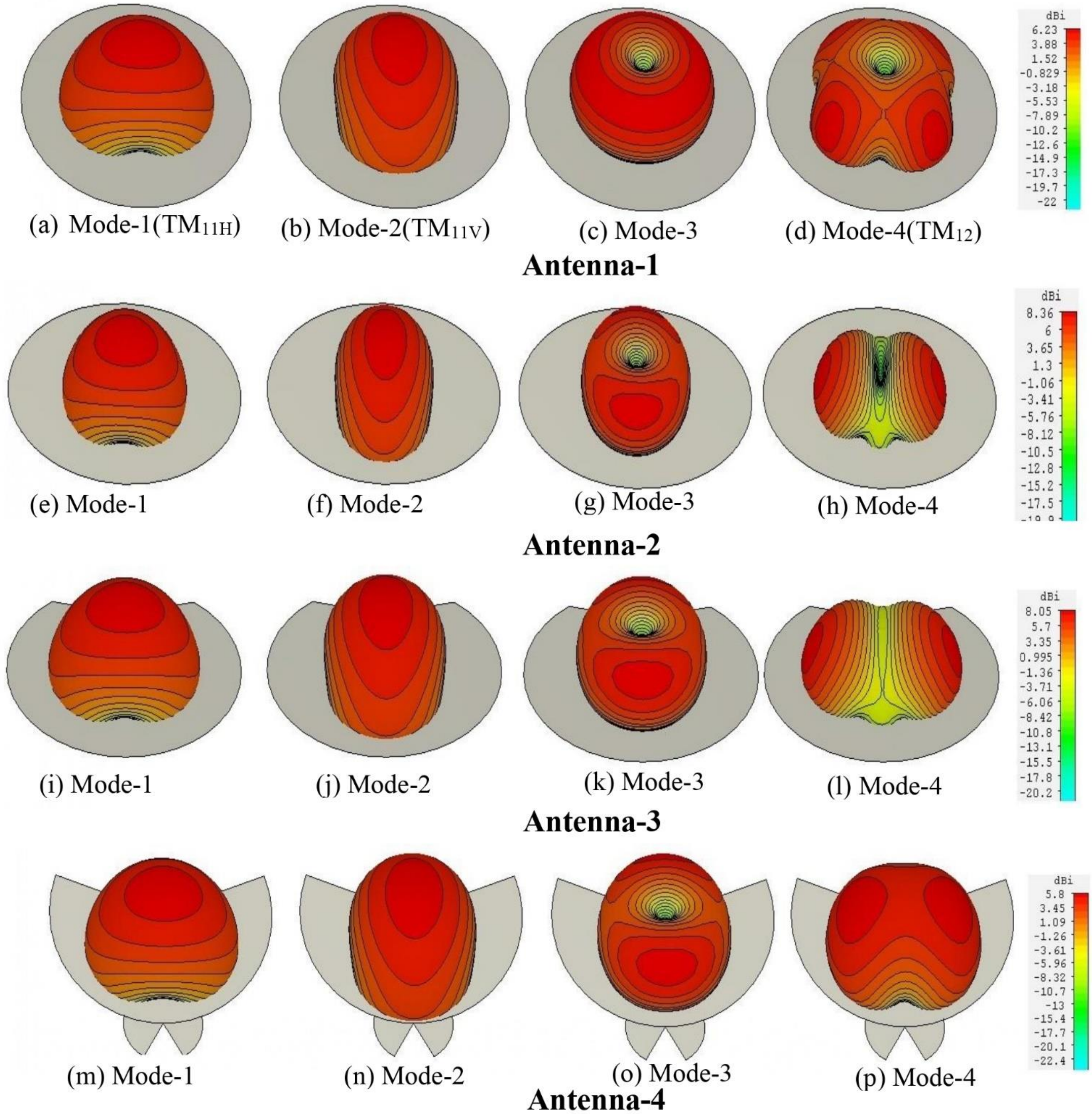

Figure 5. Far-field radiation patterns of antennas

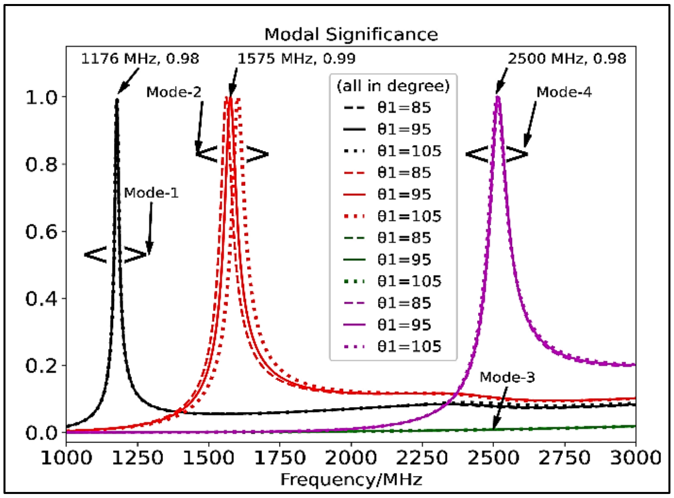

Figure 6. Antenna-2 parametric study MS plot

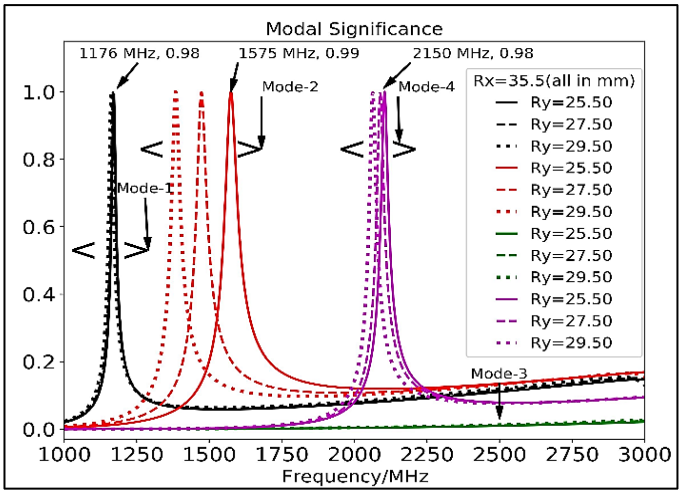

Figure 7. Antenna-3 parametric study MS plot

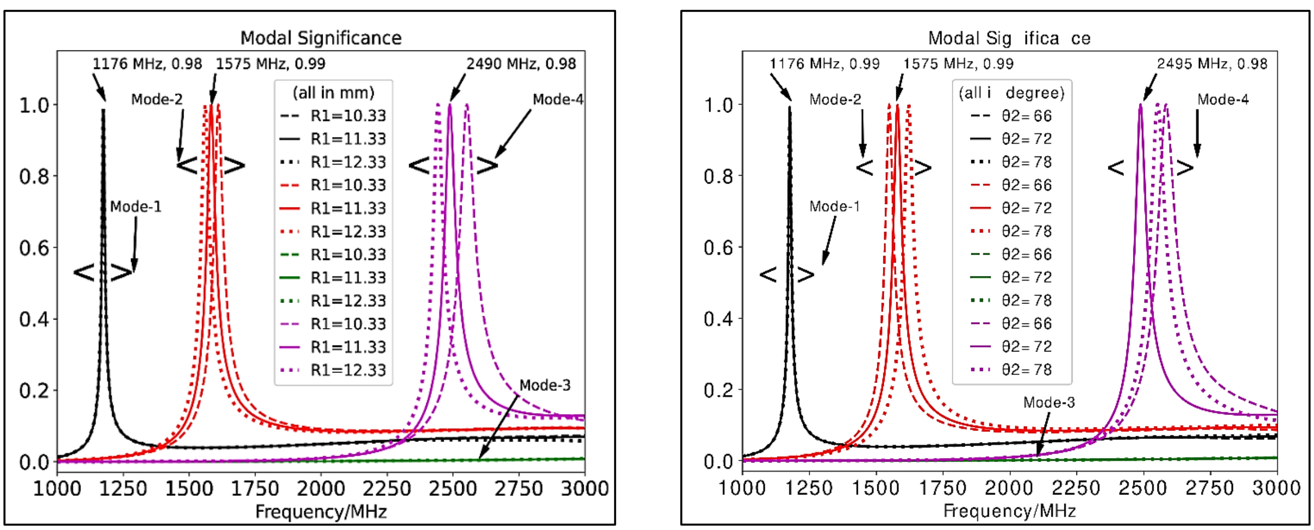

(a) Antenna-4 parametric study MS plot with *R1*

(b) Antenna-4 parametric study MS plot with *θ2*

Figure 8. Antenna-4 modal analysis

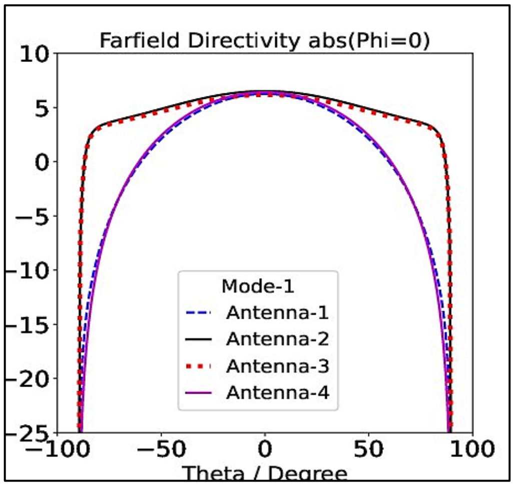

(a) Mode-1

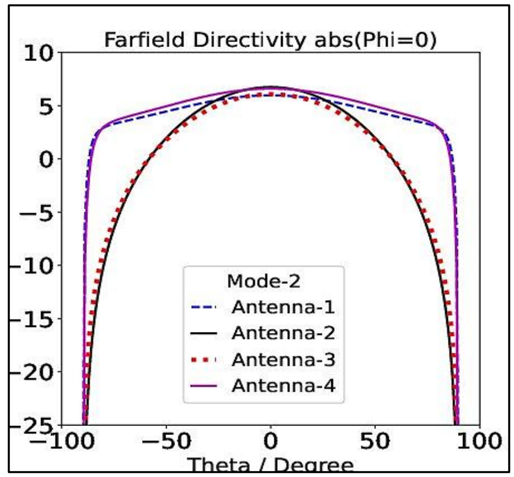

(b) Mode-2

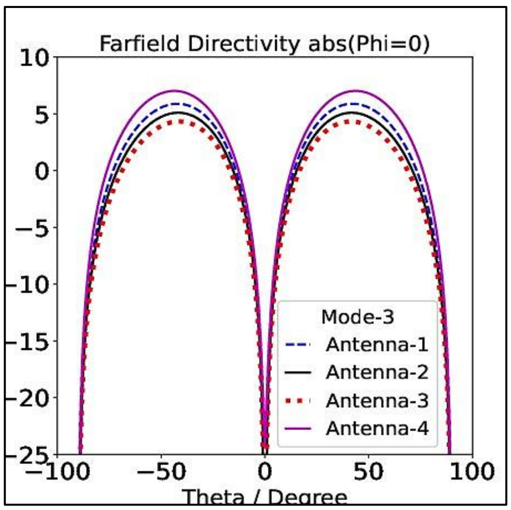

(c) Mode-3

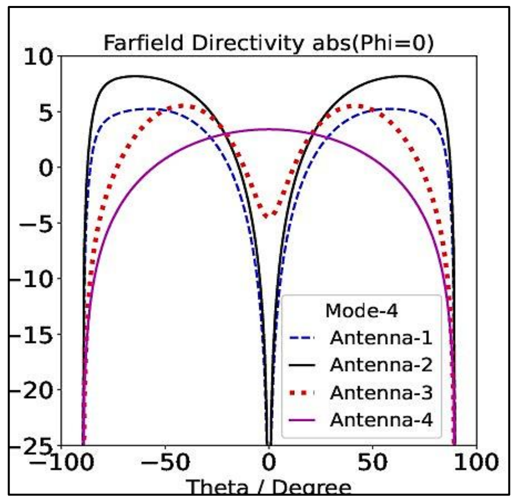

(d) Mode-4

Figure 9. Farfield radiation characteristics at Phi=0

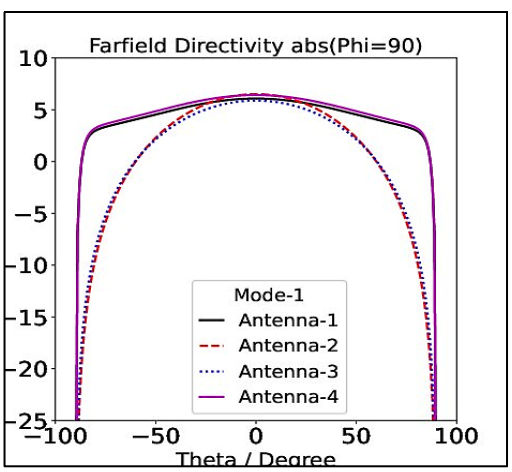

(a) Mode-1

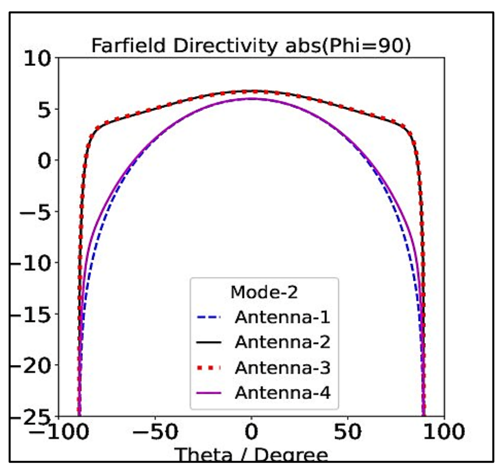

(b) Mode-2

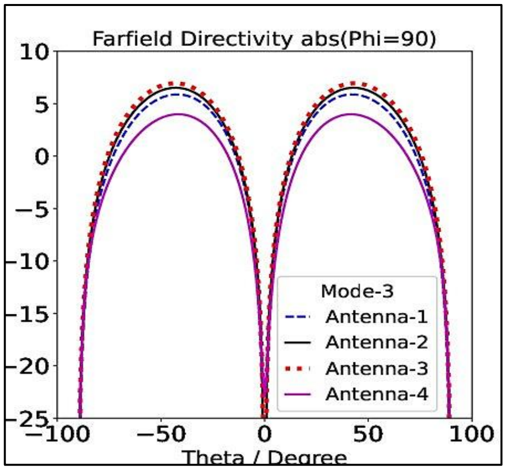

(c) Mode-3

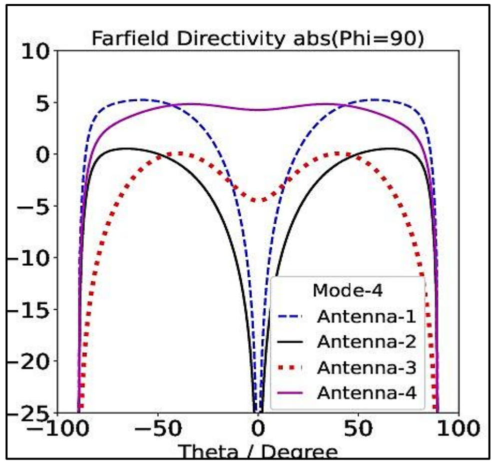

(**d)** Mode-4

Figure 10. Far field radiation characteristics at Phi=90

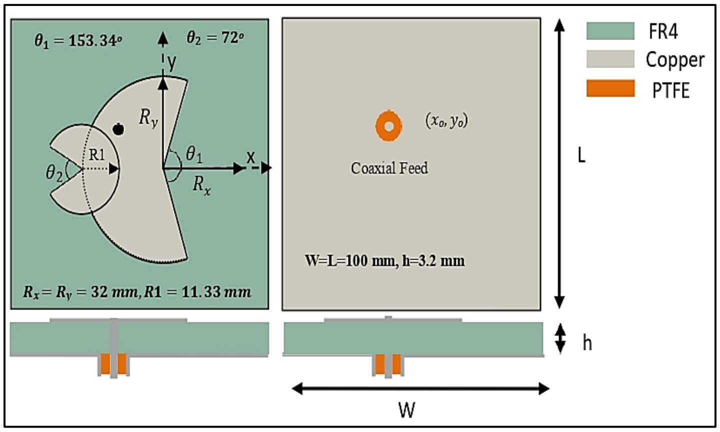

Figure11. Geometry of proposed tri-band antenna

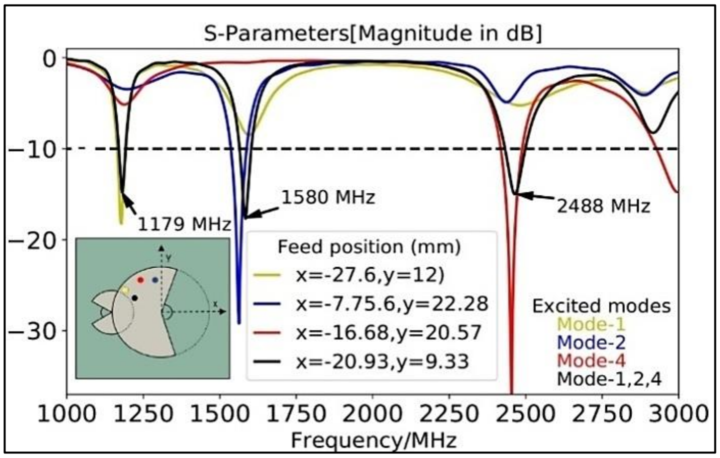

Figure 12. S_{11} plot for modes excitation with feed

Figure 13. Photograph of the fabricated layout of

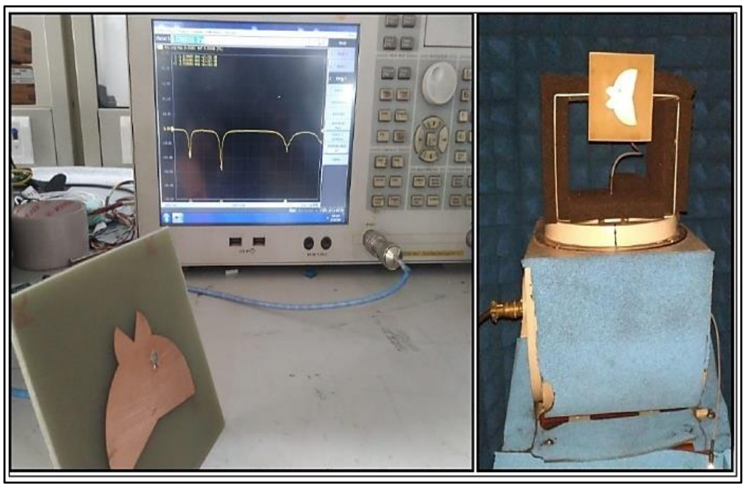

Figure 14. S_{11} and radiation pattern measurement set-up of proposed antenna the proposed antenna

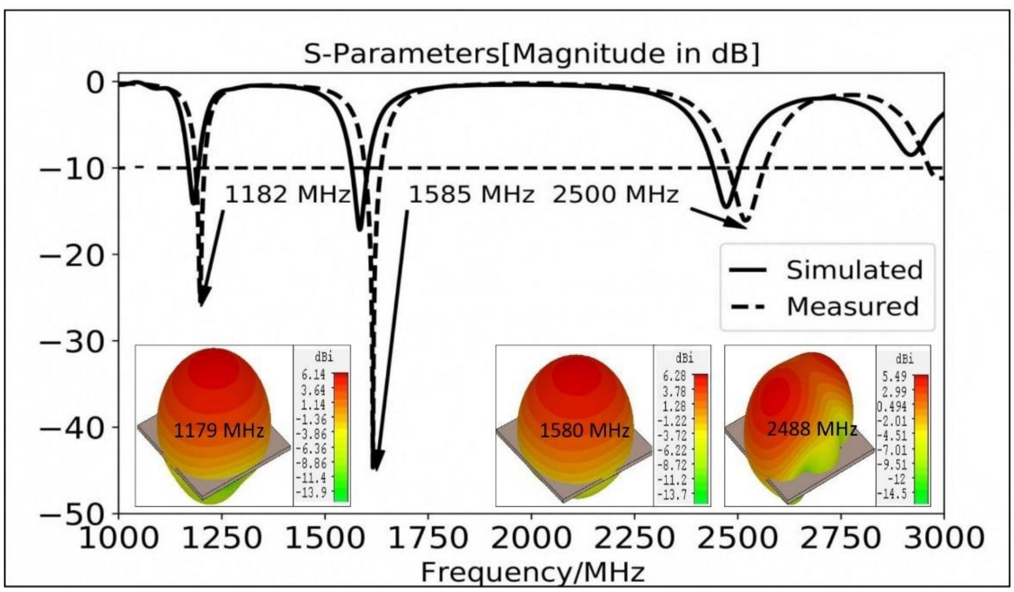

Figure 15. Scattering Parameter (S_{11}) of antenna

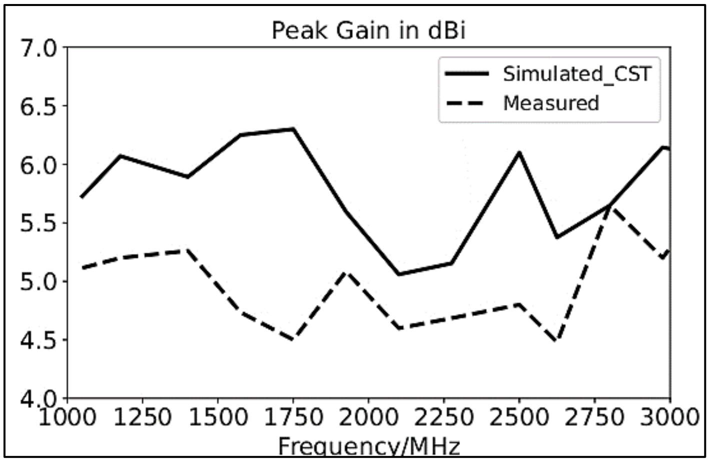

Figure 16. Simulated and measured peak gain

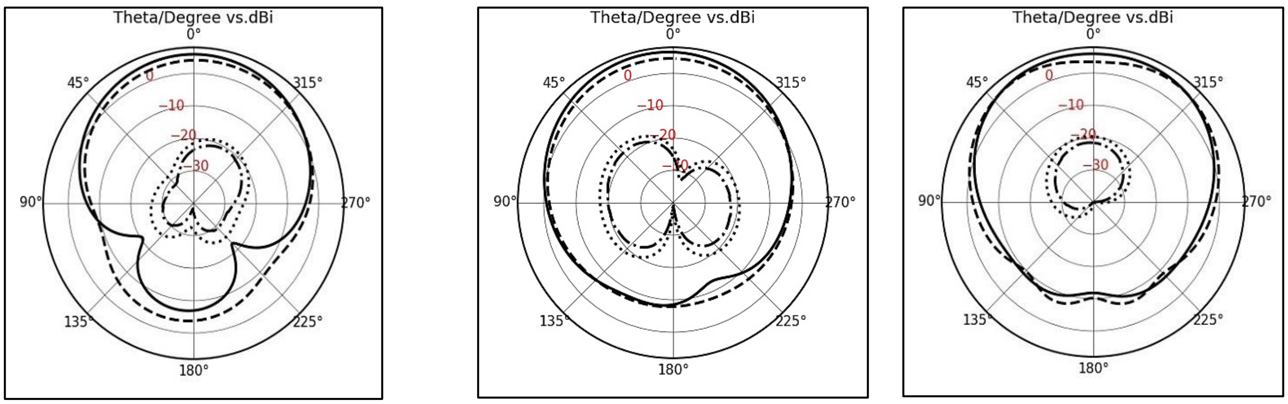

(a) $\phi = 90^0$, 1174 MHz **(b)** $\phi = 90^0$, 1575 MHz **(c)** $\phi = 90^0$, 2495 MHz

(d) $\phi = 0^0$, 1174 MHz **(e)** $\phi = 0^0$, 1575 MHz **(f)** $\phi = 0^0$, 2495 MHz

Figure 17. The proposed antenna's measured and simulation-based radiation pattern
{Solid line Co-pol (Simulated), Dash line Co-pol (Measured),
Square dot line Cross-pol (Simulated), Dash Dot Cross line pol (Measured)}

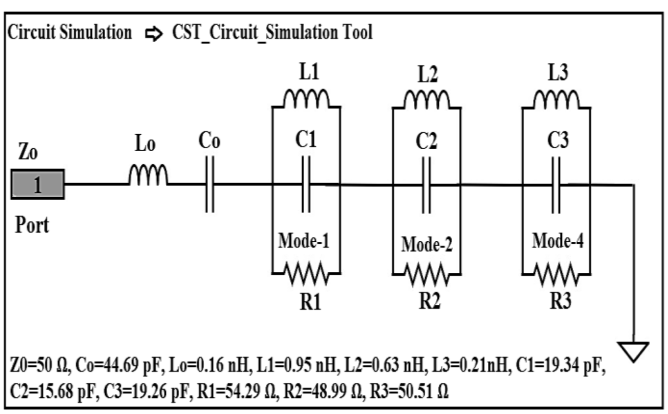	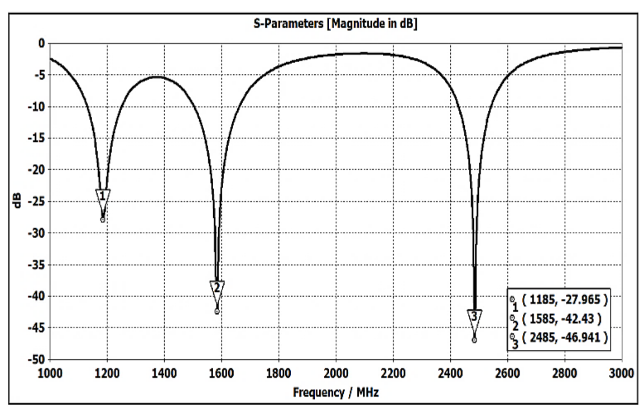
(a)	(b)
Figure 18. (a) Equivalent Circuit Modeling (ECM) analysis	(b) S_{11} of ECM of proposed antenna

TABLE 1 Comparison of proposed approach with previous work.

Ref.	Multi-band Methodology	Enhancement of higher-order mode Methodology	Resonant-mode (Frequency MHz)	Volume (mm^3)	Material	Complexity	Peak gain (dBi)
[1]	Adding shorting pins and slots	A narrow slot with differential feed	2 (3600, 5900)	100*100*2	F4B	High	10.2, 10
[2]	assembling the patch's shorting pins and slot	differential feeding with shorting pins and slots	3 (3900, 4950, 5900)	110*90*1.58	Rogers5880	High	10, 10.4,10.2
[3]	Exciting TM_{010} and TM_{030} modes	putting a mu-negative or double-negative metamaterial into operation	2 (903, 1796)	120*150*5	MNG or DNG	High	5.19, 7.47
[5]	not reported	narrow slot at the patch center	2 (1800)	330*330*1.54	not reported	Simple	7
[6]	not reported	Embedded narrow slot at patch center	1 (1000)	not reported	Arlon diclad 527	Simple	13
This Work	Excitation of two orthogonal modes and one higher order mode	Surface current nulls (out-of-phase nulls) shifting toward the patch corners by re-shaping the antenna structure	3 (1182, 1585, 2500)	100*100*3.2	*FR-4*	Simple	5.2, 4.6, 4.2

Indra Bhooshan Sharma received B.Tech in 2013 from JNIT, Jaipur, India. He did M.Tech in 2016 from GECA, Ajmer, India and presently, he is PhD scholar from MNIT, Jaipur, India. He joined as Guest Faculty in the Department of ECE, MNIT, Jaipur in 2016 and designated as an PA-III in the CSIR-CEERI, Pilani in 2018. He is an active Member of IEEE including Antenna and Propagation Society. He is the author/coauthor of more than 30 research papers published in the refereed international/ national journals and conferences. His research interest includes planar UWB antennas, circularly polarized antennas, Reconfigurable antennas, and microwave absorber, and so forth.

Prachi Joshi received B.Tech in Electronics and Communication Engineering from Govt. Women Engineering College, Ajmer, India (2015). She is pursuing M.Tech degree from Malaviya National Institute of technology, Jaipur since 2022. Her research interests include planar Micro strip antenna, UWB antennas, circularly polarized antennas, Reconfigurable antennas etc.

Subhash Shrimal received the B.E. degree in Electronics and communication engineering from the University of Rajasthan, Jaipur, India in 2005 and the M.Tech. degree in Electronics and communication engineering from Malviya

National Institute of Technology, Jaipur, India in 2008. He is currently working toward his PhD degree (Part-Time) at MNIT Jaipur since 2020. He is presently working as Lecturer in Government Polytechnic College, Board of Technical Education Rajasthan. His main areas of interest are micro strip and reconfigurable planar antennas.

Bhawna Kalra (Member IEEE) received B.tech degree from RTU kota in 2013, master's degree from UCE RTU Kota in 2016 and Pursuing Phd from MNIT Jaipur. She is currently working as assistant professor in JECRC Foundation Jaipur. Her area of research Includes Circularly polarized patch antenna, Shared aperture antenna, Phased array antenna and antennas for 5G applications.

Mahendra Mohan Sharma received BE in 1985 from NIT, Srinagar, India. He did M.Tech from IIT, Delhi and PhD from MNIT, Jaipur, India. He joined as Lecturer in the Department of Electrical Engineering, MNIT, Jaipur in 1986 and designated as an Associate Professor there in 1995. Presently, He is working as Professor with the Department of Electronics and Communication Engineering, MNIT Jaipur. Besides being an able academician and administrator (Registrar in MNIT and Ex Executive Director at National Institute of Electronics and Information Technology, Chandigarh). He is an active member of IEEE, Member, Broadcasting Engineering Society (India) and Life Senior Member ISTE professional bodies. He is Honorary Secretary, IEEE-MTTS India Council Chapter. He is the author/coauthor of more than 100 research papers published in international/national journals and conferences. His research interests include design and modeling of antennas, array, and FSS.